# Spin reorientation transitions of Ni/Pd(111) films induced by Fe deposition

Isamu Yamamoto,[1] Takeshi Nakagawa,[1,2] Yasumasa Takagi,[1,2] and Toshihiko Yokoyama[1,2,*]
[1]*Department of Materials Molecular Science, Institute for Molecular Science, Myodaiji-cho, Okazaki 444-8585, Japan*
[2]*The Graduate University for Advanced Studies (SOKENDAI), Myodaiji-cho, Okazaki 444-8585, Japan*
(Received 13 April 2010; revised manuscript received 17 May 2010; published 25 June 2010)

Two opposite spin reorientation transitions (SRTs) of Ni/Pd(111) films induced by Fe-capping layers have been investigated *in situ* by low-energy electron diffraction, magneto-optical Kerr effect, and x-ray magnetic circular dichroism (XMCD). In pure Ni films grown on Pd(111), no thickness-driven SRT was observed, leaving the magnetization easy axis in plane. Deposition of Fe 1 monolayer (ML) on Ni(6 ML)/Pd(111) causes a transition to perpendicular magnetization, and further Fe 3 ML deposition leads to a return to in-plane magnetization. The XMCD results confirm a contribution of the orbital magnetic moment of a single Fe layer to the first SRT, which gives a significant impact on the Fe-Ni interface that stabilizes perpendicular magnetic anisotropy (PMA). The second SRT coincides with the structural change in the Fe film from the fcc to bcc phase, where the reduction in the orbital magnetic moment along the perpendicular direction to suppress the PMA stability was observed. It can be proposed that the origin of the second SRT to in-plane magnetization is attributed to cooperative contributions of the structural transformation of the Fe film and the enhanced demagnetizing field.

DOI: 10.1103/PhysRevB.81.214442 PACS number(s): 75.70.−i, 75.30.Gw, 78.20.Ls

## I. INTRODUCTION

Magnetic anisotropy of magnetic materials has widely been investigated in last decades.[1–6] Especially perpendicular magnetic anisotropy (PMA) has attracted much interest for fundamental physics as well as technological applications. If one consider only classical magnetic dipole-dipole interaction of demagnetizing field, magnetic thin films always favor in-plane magnetization. However, since the magnetization easy axis is also influenced by surface, interface, and volume elastic strains of the films, magnetic thin films and multilayers often exhibit PMA.[7–10] Moreover, surface modifications of magnetic thin films such as adsorption of molecules and metals sometime induce drastic transitions of the change in the magnetization easy axis,[11–13] known as a spin reorientation transition (SRT).

Recently the SRTs induced by Fe deposition have been observed in Fe/Co/Pd(111).[13] Submonolayer Fe deposition on the in-plane magnetized Co/Pd(111) film causes a SRT to PMA. Further deposition of Fe induces another SRT to in-plane magnetization. They suggested that the first SRT is attributed to huge PMA of the Fe-Co interface. However, they could not exclude a possibility that the Fe atoms form three-dimensional islandlike clusters, which might lead to large PMA.[14,15] It is thus interesting to investigate whether single-layer Fe on other fcc(111) surface also shows huge PMA or not. This is one of the reasons why we have chosen the Fe/Ni/Pd(111) system in this work.

Fe-induced twice SRTs have also been observed for Fe/Ni bilayers.[16–19] Most researchers reported that the SRT to PMA caused by submonolayer ($<0.5$ ML) Fe deposition and suggested that the first SRT is attributed to large PMA of the Fe-Ni interface. However, the critical thickness of Fe for the second SRT to in-plane magnetization somewhat varies depending on the systems. Abe *et al.*[16] performed x-ray magnetic circular dichroism (XMCD) measurements of the Fe/Ni/Cu(001) system, and reported that the second SRT induced by 1–2 ML Fe deposition. Ramchal *et al.*[17] also reported the critical Fe thickness of $2.7 \pm 0.2$ ML for Ni/Cu(001), which was evaluated by spin-polarized low-energy electron microscopy (SPLEEM). Thamankar *et al.*[18] studied the Fe/Ni/Cu(001) system by the magneto-optical Kerr effect (MOKE), and suggested that the Fe/Ni bilayer shows in-plane magnetization after growing more than 2.5 ML Fe. Sander *et al.*[19] investigated the Fe/Ni/W(110) system by low-energy electron diffraction (LEED), angle-resolved Auger electron spectroscopy (AR-AES), and MOKE. They claimed that the second SRT occurs at 4 ML Fe, where the structural transition takes place from the fcc to bcc phase. The relation between the second SRT and the structural change in the Fe film has, however, not been investigated so far.

In this study, we have investigated the structural and magnetic properties of the Fe/Ni bilayer on Pd(111) by *in situ* characterization techniques as LEED, MOKE, and XMCD. The magnetic-anisotropy constants estimated from the magnetization curve and orbital magnetic moments are discussed with the structure of the Fe films. The estimated magnetic-anisotropy constants may indicate the origins of the SRTs for the Fe/Ni/Pd(111) system.

## II. EXPERIMENTS

MOKE and XMCD measurements were performed *in situ* using different ultrahigh vacuum (UHV) chambers. Both the systems have been reported previously.[20,21] Briefly, they are equipped with reflection high-energy electron diffraction and LEED optics, and the LEED equipments were also used to record AES. The MOKE experiments were performed with a laser diode (635 nm) and an electromagnet (maximum magnetic field of ~3000 Oe) at room temperature (RT). The incident angle of the laser was 45° from the surface normal (0°) for both longitudinal and polar configurations. The XMCD measurements were done using a system (JANIS: 7THM-ST-UHV) with a superconducting magnet (7 T) and a

 

liquid He cryostat (~3.8 K) at Beamline 4B in UVSOR-II of Institute for Molecular Science.[20–22] The circularly polarization factor ($P_c$) of x rays was evaluated at ~0.67, where the energy resolution $E/\Delta E$ was 800 at $E=800$ eV. We took the x-ray absorption spectra (XAS) by monitoring the total electron yield, measuring simultaneously the intensity of incident x rays with a Au-coated W mesh placed in front of the sample. The XMCD spectra were recorded with reversal of the magnetic field at x-ray incidence angles $\theta_i$ of 0° (surface normal) and 55° (grazing). The XMCD measurements were done at a temperature of $T=55$ K.

A Pd(111) single crystal was cleaned by repeated cycles of $Ar^+$ sputtering at 1.5 keV and subsequent annealing at 900 K. The cleanness was checked by AES (typical contaminations of C and O), and the LEED showed a sharp $1\times1$ pattern with low background. Ni and Fe thin films were deposited by the electron-beam evaporation method at RT. The deposition rates of both Ni and Fe were ~0.5 ML/min, which were monitored by the ion current measurement during depositions and were calibrated for each chamber by using Ni/Cu(001) and Fe/Cu(001) as reference samples. After the deposition, the deposited amounts were further verified by the AES and/or the x-ray absorption intensities of Fe, Ni, and Pd. Note that all the XMCD and MOKE measurements were performed *in situ* without any capping layer deposited on the sample surface. In the XMCD measurement chamber, the pressure at the sample position is expected to be extremely good due to the environment of the surrounding liquid He reservoir of the superconducting magnet, though the exact pressure cannot be measured. Moreover, the measurement temperature was 5 K, and residual water that adsorbs on the surface does not oxidize the Fe surface due to much larger activation energy than the thermal energy. In the MOKE chamber, the measurement period was sufficiently short. No oxidation effect is therefore expected during the present *in situ* measurements.

## III. RESULTS AND DISCUSSION

### A. Structural properties

LEED patterns of clean Pd(111), Ni(3 and 6 ML)/Pd(111), and Fe(1–5 ML)/Ni(6 ML)/Pd(111) are shown in Fig. 1. Upon Ni deposition on Pd(111), in addition to sharp fundamental spots from the substrate, Moiré patterns were observed up to ~6 ML, as shown in the magnified part of Fig. 1(c). The periodicity of the Moiré patterns is 11 times as large as that of clean Pd(111). This result is consistent with the lattice mismatch between Ni (2.49 Å) and Pd (2.75 Å) of 9.1%.[23] The large lattice mismatch impedes a pseudomorphic growth but the Ni films are grown epitaxially since the LEED patterns show threefold symmetry as expected for fcc Ni(111). Although we have not observed scanning tunnel microscopy images of the present sample, the sharpness of the LEED superstructure indicates that the film grows in a layer-by-layer fashion (though it may not be perfect) rather than a island growth mode. Similar Moiré patterns have been observed for Co/Pd(111) [Refs. 13 and 24] and Pd/Ni(111) [Refs. 23 and 25] but not been observed for Ni/Pd(111) [Refs. 25 and 26]. We guess that this may be ascribed to some different deposition conditions in the present sample preparation from those of Refs. 25 and 26.

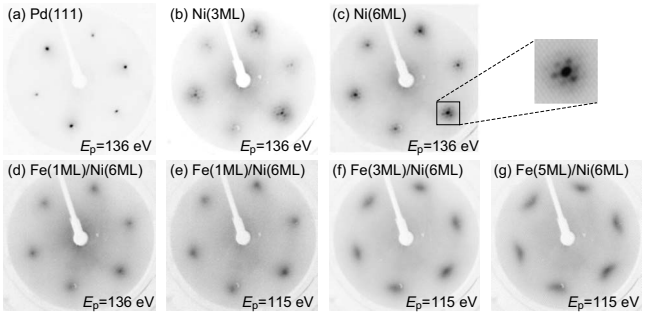


FIG. 1. LEED patterns of Fe/Ni/Pd(111) taken with a primary electron energy of $E_p=136$ or 115 eV: (a) bare Pd(111), (b) Ni(3 ML)/Pd(111), (c) Ni(6 ML)/Pd(111), (d) and (e) Fe(1 ML)/Ni(6 ML)/Pd(111), (f) Fe(3 ML)/Ni(6 ML)/Pd(111), and (g) Fe(5 ML)/Ni(6 ML)/Pd(111). The marked area in (c) is magnified on the right-hand side.

After deposition of 1 ML Fe on Ni(6 ML)/Pd(111), the LEED spots become broader and the LEED patterns show sixfold symmetry with no satellite spots as in Fig. 1(d). Although these changes are found, the LEED pattern is essentially the same, suggesting a pseudomorphic epitaxial growth of Fe at the initial stage, in contrast to incoherent growth of Ni on Pd(111). This is because there is almost no mismatch between Ni and Fe (2.48 Å).[13] The lack of threefold symmetry indicates that there are some stacking domains of fcc Fe(111), as reported by Johnston *et al.*[27]

With further Fe deposition, the LEED patterns taken at 136 eV are gradually fading away, and the LEED spots at 115 eV become elongated compared to those of Fe 3 ML. The change in the LEED patterns indicates the structural change in the Fe film around 3 ML. It is well known that a structural transition of Fe films grown on fcc(111) substrates occurs from a pseudomorphic fcc phase to bcc. Previous experimental studies have shown that Fe grows pseudomorphically up to 1–3 ML and is subsequently transformed into the bcc(110) phase with the Nishiyama-Wassermann (NW) or Kurjumov-Sachs (KS) orientation.[27–30] Johnston *et al.*[27] investigated the growth of the Fe film on a fcc Ni(111) film of Ni(2 ML)/W(110), by LEED and AR-AES. They reported that a slightly distorted fcc(111) structure grows up to 3 ML, after which a transition to the bcc structure with KS orientation occurs. Gazzadi *et al.*[28] suggested a pseudomorphic growth with fcc structure of the Fe films on Ni(111) single crystals up to 2 ML and a subsequent transition to the bcc phase with NW orientation between 3 and 6 ML. An *et al.*[29,30] observed similar elongated LEED spots in 3.2–4.2 ML Fe films on the Ni(111) single crystal. The quality of their LEED patterns is higher than that in the present work, which may be ascribed to underlying ideal structure of the Ni(111) single crystal. They suggested that the three satellite spots result from the epitaxial growth of bcc(110) on fcc(111) with the NW orientation relationship, and the structural transition of the Fe film from fcc to bcc occurs at 2 ML Fe. Therefore, we can recognize that in the present Fe/Ni/Pd(111) system, Fe grows in a layer-by-layer fashion as well rather than in a island growth mode, and that the structural

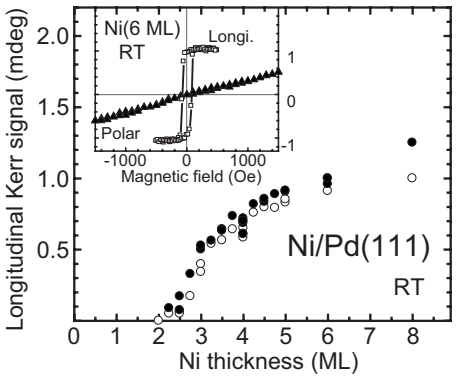


FIG. 2. Longitudinal MOKE rotation angles of Ni/Pd(111) at RT as a function of Ni thickness. Remanent (○) and saturated (●) magnetizations along the in-plane direction are plotted. The inset shows the magnetization curve of Ni(6 ML)/Pd(111) (□), together with the polar MOKE one (▲).

change in the Fe film from fcc to bcc occurs at ~3 ML, although we could not determine the NW or KS orientation.

### B. MOKE results: Spin reorientation transition

Figure 2 shows the magnetization of Ni/Pd(111) at RT as a function of Ni thickness recorded with the longitudinal MOKE measurements. The plots correspond to in-plane remanent and saturated magnetizations as a function of Ni-film thickness. The inset shows the magnetization curves of Ni(6 ML)/Pd(111). The Ni films show only in-plane magnetizations with no perpendicular component. Thus the magnetization easy axis of the Ni/Pd(111) films is in plane. No thickness-driven SRT is found for Ni/Pd(111). A hysteresis along the magnetization easy axis (in plane) appear in the films thicker than ~2 ML. The critical thickness for the ferromagnetic order at RT is similar to those for Ni(111) films on other substrates: 2.5 ML on Cu(111),[31] 2 ML on W(110),[32] and 2.0–2.4 ML on Re(0001).[33] In Ni(2 ML)/Pd(111), the Curie temperature is found to be ~210 K estimated from the temperature-dependent MOKE measurement (not shown). It is also noted that the Ni/Pd(111) films with thickness below 6 ML shows 100% remanent magnetization, indicating the formation of well-extended films (not island formation). On the other hand, the square loops gradually become slanted above 6 ML, where the Moiré patterns are fading away. This suggests that the Ni film thicker than 6 ML becomes disordered, and the various magnetic domains are formed.

By depositing Fe, two opposite SRTs were observed. Figures 3(a) and 3(b) show the magnetization curves of a wedged Fe film (0–4 ML) on Ni(6 ML)/Pd(111) at RT, recorded with the longitudinal and polar MOKE measurements. The MOKE rotation angles measured in remanence as a function of Fe thickness are also shown in Fig. 3(c). By depositing submonolayer Fe, a remanent polar Kerr signal was detected. An increase in the remanent polar Kerr intensity up to ~2 ML Fe is found while the remanent longitudinal Kerr signal disappears above 1 ML Fe. Therefore, the magnetization easy axis completely changes from in plane to

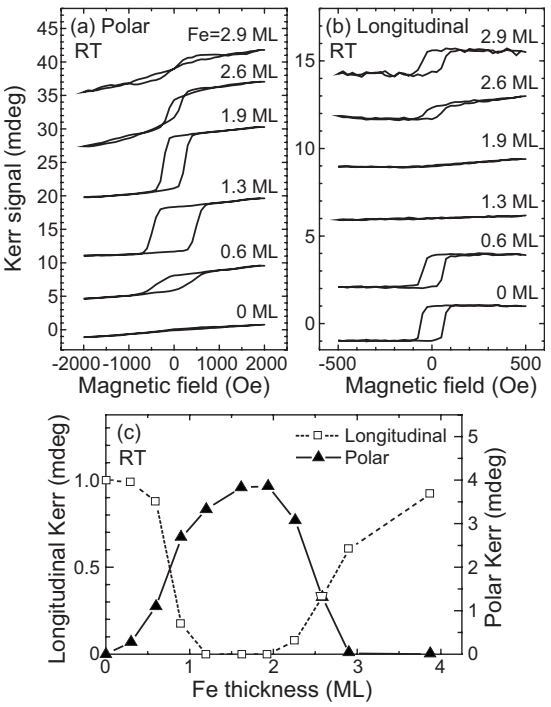


FIG. 3. (a) and (b) Magnetization curves of a wedged Fe film on Ni(6 ML)/Pd(111) at RT recorded with the (a) polar and (b) longitudinal MOKE measurements. (c) The polar (▲) and longitudinal (□) Kerr intensities measured in remanence as a function of Fe thickness.

perpendicular around 1 ML Fe. With further Fe deposition, above 2 ML, the longitudinal Kerr signal appears again, and the remanent polar Kerr intensity becomes weaker. The second SRT from perpendicular to in plane occurs at ~3 ML, where the structural change in the Fe film from fcc to bcc takes place.

The twice SRTs, in-plane to perpendicular magnetization and vice versa, induced by Fe deposition have been observed for Co/Pd(111),[13] Ni/Cu(001),[16–18] and Ni/W(110).[19] The previous experimental studies have shown that the first SRT to perpendicular magnetization occurs below 0.5 ML Fe and that the Fe-Ni and Fe-Co interfaces have large magnetic anisotropy that favors perpendicular magnetization. Although the appearance of the polar Kerr signals with submonolayer Fe deposition in the present system is consistent with the previous works, some remanent longitudinal Kerr signals remain even up to ~0.9 ML Fe. It is supposed that the PMA of the Fe-Ni interface of the present Fe/Ni/Pd(111) system is smaller than the other systems. For submonolayer and 2–3 ML Fe regions, during the SRTs, both the polar and longitudinal Kerr intensities were detected, indicating either cant magnetization or mixed magnetic domains. Although we cannot give a conclusion to the magnetization configuration during the SRTs, the slow SRTs might imply the cant magnetization. In fact, the cant magnetization during the slow SRT has observed for the Fe/Ni/Cu(001) system as reported by Ramchal *et al.*,[17] although their SPLEEM measurements were performed without applying a magnetic field.

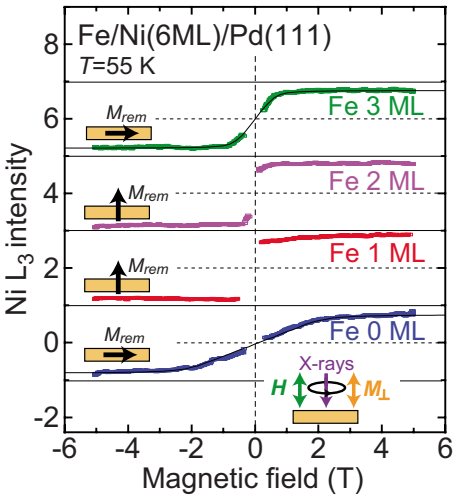


FIG. 4. (Color online) The magnetization curves of Fe/Ni(6 ML)/Pd(111) at $T=55$ K along the surface normal ($\theta_i=0°$), recorded with the Ni $L_3$ intensity. The curves are shifted along the $y$ axis in an interval of +2. The directions of remanent magnetization, the magnetization easy axis, are also depicted. The thin solid lines are the simulated magnetization curves using Eq. (1), the classical Boltzmann distribution, and the Monte Carlo method.

### C. XMCD results: Magnetic anisotropy

We have performed XMCD measurements in order to clarify the origins of the SRTs induced by Fe deposition. Figure 4 shows the magnetization ($M$-$H$) curves of Fe/Ni(6 ML)/Pd(111) at $T=55$ K along the surface normal ($\theta_i=0°$), recorded with the Ni $L_3$ intensity. The data at a low magnetic field (from −0.5 to +0.5 T) were omitted because of the presence of huge spikes in a low magnetic field region, where some photoelectrons emitted once from the sample return back to the sample holder due to a large radius of the cyclotron motion. Although the $M$-$H$ curves recorded with the Fe $L_3$ intensity have also measured (not shown), the behaviors are found to be essentially the same as that for the Ni $L_3$ edge. The magnetization easy axes of the films are consistent with the MOKE results. The $M$-$H$ curves along the hard axis provide information on magnetic-anisotropy constants and are useful to estimate the saturated magnetization that is required in the XMCD analysis. The magnetic field of ±5 T were confirmed to be sufficient for saturating magnetization even along the hard axis.

The analysis of the $M$-$H$ curve permits to estimate a magnetic-anisotropy energy (MAE) by using a simple second-order magnetic-anisotropy model. Assuming a magnetic-anisotropy constant $K_u$, the MAE $E_a$ is phenomenologically expressed as

$$E_a = \left(\frac{M_s^2}{2\mu_0} - K_u\right)\cos^2\theta_M - \mathbf{M}_s \cdot \mathbf{H}, \tag{1}$$

where $M_s$ is the saturated magnetization obtained by the following XMCD analysis, $\mu_0$ the permeability of vacuum, **H** the applied magnetic field, and $\theta_M$ the angle between $\mathbf{M}_s$ and **H**. The simulated results for the Fe 0 and 3 ML films are also depicted in Fig. 4, and the resultantly obtained uniaxial magnetic-anisotropy constants $K_u$ are −40 and 20 $\mu$eV/atom for the Fe 0 and 3 ML films, respectively. The corresponding anisotropic magnetic fields $H_a$ are estimated to be 2.6 T and 0.8 T, respectively. Note here that $K_u$ for Fe(3 ML)/Ni(6 ML)/Pd(111) is positive, implying that perpendicular magnetization is still favored. The estimated $K_u$ of +20 $\mu$eV/atom is, however, too small to overcome the negative contribution of the demagnetizing-field effect (−51 $\mu$eV/atom), resulting in in-plane magnetization. The estimated parameters are listed in Table I.

The XMCD analysis procedure has been described previously.[20,21,34] Briefly, Fig. 5 depicts the examples of the Ni $L_{3,2}$- and Fe $L_{3,2}$-edge circularly polarized XAS, $\mu^+$ and $\mu^-$, taken at $\theta_i=0°$ (surface normal x-ray incidence). $\mu^+$ and $\mu^-$ denote those for the x-ray helicities parallel and antiparallel to the electron spins in the specimen, respectively. The spectra are obtained from linear background subtraction and subsequent normalization with the edge jump at a certain postedge energy. In the case of thick films, the self-absorption effect should be corrected since the x-ray penetration depth is not sufficiently large compared to the electron escape depth.[35] In the present self-absorption correction, uniformly flat films were assumed. The XMCD spectra are given as a difference of the two self-absorption corrected XAS and the normalization with a circularly polarization factor.

TABLE I. Results of the anisotropic orbital $m_{orb}(\mu_B)$ and isotropic-spin $m_{spin}(\mu_B)$ magnetic moments for Ni and Fe at $T=55$ K and $H=5$ T, obtained by the Ni $L$- and Fe $L$-edge XMCD analysis for Fe/Ni(6 ML)/Pd(111) films. The resultant uniaxial magnetic-anisotropy constants $K_u$ (meV/atom) are tabulated, which are obtained from the Bruno model. For the Fe 0 and 3 ML films with the in-plane magnetization easy axes, the uniaxial magnetic-anisotropy constants $K_u$ (meV/atom) and the corresponding anisotropy fields $H_a$ (T), which are obtained from the $M$-$H$ curve analysis, are also given. The values in parentheses are estimated errors in the XMCD analysis, which are effective for the last digit of the obtained quantities.

| Fe (ML) | Ni $L$ | | | Fe $L$ | | | Bruno | $M$-$H$ | |
|---|---|---|---|---|---|---|---|---|---|
| | $m_{spin}$ | $m_{orb}^{\parallel}$ | $m_{orb}^{\perp}$ | $m_{spin}$ | $m_{orb}^{\parallel}$ | $m_{orb}^{\perp}$ | $K_u$ | $K_u$ | $H_a$ |
| 0 | 0.74(7) | 0.10(1) | 0.09(1) | | | | −0.031 | −0.040(5) | 2.6(1) |
| 1 | 0.77(7) | 0.08(1) | 0.11(1) | 2.42(24) | 0.15(1) | 0.22(2) | 0.084 | | |
| 2 | 0.74(7) | 0.07(1) | 0.13(1) | 2.59(26) | 0.22(2) | 0.34(3) | 0.172 | | |
| 3 | 0.74(7) | 0.08(1) | 0.07(1) | 2.34(23) | 0.12(1) | 0.17(2) | 0.014 | 0.020(5) | 0.8(1) |

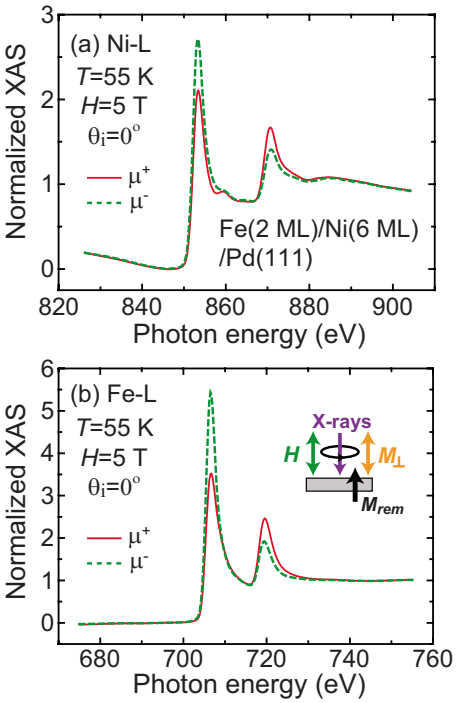


FIG. 5. (Color online) (a) Ni $L_{3,2}$-edge and (b) Fe $L_{3,2}$-edge circularly polarized XAS, $\mu^+$ (solid line) and $\mu^-$ (dashed line), taken at $\theta_i=0°$ (surface normal), $T=55$ K, and $H=\pm 5$ T. $\mu^+$ and $\mu^-$ denote those for the x-ray helicities parallel and antiparallel to the electron spins in the specimen, respectively.

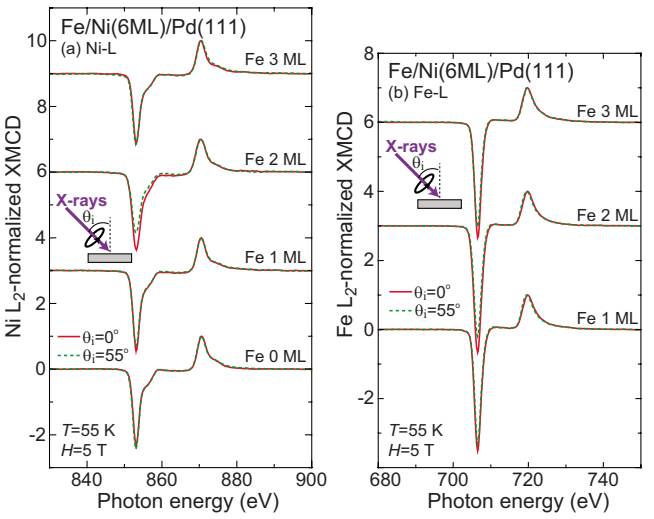


FIG. 6. (Color online) Angular-dependent (a) Ni $L_{3,2}$-edge and (b) Fe $L_{3,2}$-edge XMCD spectra for Fe/Ni(6 ML)/Pd(111) at $T=55$ K and $H=\pm 5$ T for the x-ray incident angles $\theta_i=0°$ (solid line) and $\theta_i=55°$ (dashed line). All the XMCD spectra are normalized at the $L_2$-edge peak top.

The XMCD sum-rule analysis is subsequently performed using the formulas of the orbital magnetic moment $m_{\mathrm{orb}}$ and the spin magnetic moment $m_{\mathrm{spin}}$. The $3d$ hole number $n_{\mathrm{d}}$ was estimated from the relative intensities of the Fe and Ni $L_{3,2}$ white lines. Here the reference samples were used for the calibration of the absolute values: $n_{\mathrm{d}}=1.5$ and 3.4 for bulk-like Ni and Fe, respectively. The orbital magnetic moment $m_{\mathrm{orb}}$ and the effective spin magnetic moment $m_{\mathrm{spin}}^{\mathrm{eff}}=m_{\mathrm{spin}}+7m_{\mathrm{T}}$ ($m_{\mathrm{T}}$ the magnetic dipole moment) were resultantly obtained.

The magnetic dipole moment $m_{\mathrm{T}}$ can be estimated by using the formulas proposed by Stöhr and König[36] in the angle-dependent XMCD spectra under the saturated magnetization, although $m_{\mathrm{T}}$ obtained in the present analysis was not meaningfully large for the determination of the spin magnetic moment $m_{\mathrm{spin}}$. The formulas also permit to determine the components of the orbital magnetic moments separately along the perpendicular $m_{\mathrm{orb}}^{\perp}$ and in-plane $m_{\mathrm{orb}}^{\parallel}$ directions. We can thus evaluate all the magnetic moments using the sum rules from the XMCD data of two x-ray incident angles $\theta_i=0°$ and 55°, which are summarized in Table I.

The angular-dependent Ni $L_{3,2}$- and Fe $L_{3,2}$-edge XMCD spectra for Fe/Ni(6 ML)/Pd(111) at $T=55$ K and $H=\pm 5$ T are shown in Fig. 6. All the XMCD spectra are normalized with the $L_2$-edge peak intensity. The estimated orbital magnetic moments (see Table I) for both Ni and Fe are significantly larger than those of the corresponding bulk metals. After deposition of 1 ML Fe, the magnitude of $m_{\mathrm{orb}}^{\perp}$ and $m_{\mathrm{orb}}^{\parallel}$ of Ni is reversed. This indicates a large contribution of the Ni-Fe interface anisotropy that favors perpendicular magnetization. Similarly, $m_{\mathrm{orb}}^{\perp}$ of Fe is larger than $m_{\mathrm{orb}}^{\parallel}$. It is remarked that the orbital magnetic moments contribute to the determination of the magnetization easy axis, and that the magnetic anisotropy is dominated by the Fe-Ni interface magnetocrystalline anisotropy. It is thus concluded that the first SRT to perpendicular magnetization originates from large PMA of the Fe-Ni interface. $m_{\mathrm{orb}}^{\perp}$ of Fe further increases from Fe 1 to 2 ML, which is also consistent with the MOKE results.

When the third Fe layer is deposited, the Fe orbital magnetic moments for both the directions are drastically reduced. This drastic change in the orbital magnetic moments may be ascribed to the structural change in the Fe film. On the other hand, $m_{\mathrm{orb}}^{\perp}$ of Ni becomes smaller than $m_{\mathrm{orb}}^{\parallel}$ at 3 ML Fe deposition, indicating that the Ni film prefers in-plane magnetization. In fact, the magnetization easy axis of the Fe(3 ML)/Ni(6 ML)/Pd(111) film is in plane. It is noted that $m_{\mathrm{orb}}^{\perp}$ of Fe is slightly larger than $m_{\mathrm{orb}}^{\parallel}$, indicating that the 3 ML Fe film itself still favors perpendicular magnetization. This is consistent with the above $M$-$H$ curve analysis.

The MAE was also estimated based on the Bruno model,[1] which is theoretically derived the relation between the microscopic orbital magnetic moment and the macroscopic magnetic-anisotropy constant. According to this model, the uniaxial magnetic-anisotropy constant, $K_{\mathrm{u}}$, is proportional to the difference in the orbital magnetic moments between $m_{\mathrm{orb}}^{\perp}$ and $m_{\mathrm{orb}}^{\parallel}$ as

$$K_{\mathrm{u}}=\frac{\xi}{4}\frac{G}{H}\frac{m_{\mathrm{orb}}^{\perp}-m_{\mathrm{orb}}^{\parallel}}{\mu_B}, \tag{2}$$

where $\xi$ is the spin-orbit coupling constant, $G$ and $H$ are the integrals of the density of states. The values of $\xi$ for Ni and Fe are 52 meV and 33 meV,[37] respectively, and a rough estimation of $G/H$ is $\sim$0.2 for $3d$ transition metals.[38] The $K_{\mathrm{u}}$ value of the whole film of the Fe/Ni bilayer is estimated as a

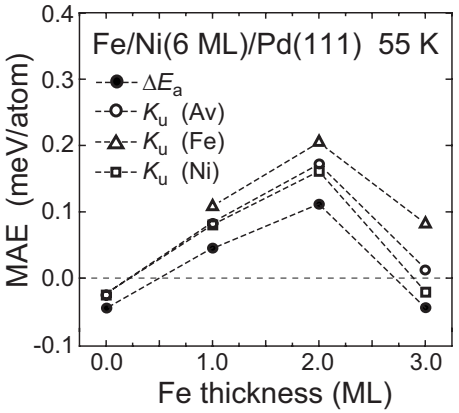


FIG. 7. Uniaxial magnetic-anisotropy constants $K_u$ estimated from the Bruno model, together with the difference of the total MAE $\Delta E_a = E_a(\theta_M = 90°) - E_a(\theta_M = 0°)$.

thickness average. The estimated $K_u$ values are plotted as a function of the Fe thickness in Fig. 7 and listed in Table I. These results are in fairly good agreement with those from the analysis of the *M-H* curves. A significant reduction in $K_u$ from 2 ML Fe to 3 ML is confirmed. This decrease may be ascribed to the structural change in the Fe film from the fcc to bcc phase. Although the $K_u$ values of Fe and the whole film are still positive possibly due to the possible strong positive contribution of the Fe-Ni interface magnetic anisotropy, the whole film shows the in-plane easy axis because of a larger negative contribution of the demagnetizing field.

The first SRT to perpendicular magnetization in the present Fe/Ni/Pd(111) system needs more Fe deposition (~1 ML) than the other systems reported previously (~0.5 ML).[13,16–19] The MAE estimated by the Bruno model is ~110 $\mu$eV/atom for Fe(1 ML)/Ni/Pd(111) while the values of ~520 and 140–230 $\mu$eV/atom were reported for Fe(1 ML)/Co/Pd(111) (Ref. 13) and Fe(1 ML)/Ni/Cu(001) (Refs. 16 and 18), respectively, which are larger than the present one. A smaller MAE of the present system may require more Fe coverage to complete the first SRT. Although there exists some difference in the transition thickness for the first SRT among the systems investigated, it can be commonly recognized that the first SRT originates from a strong positive contribution in $K_u$ from the Fe-Ni (Fe-Co) interface magnetocrystalline anisotropy.

The second SRT in the present Fe/Ni/Pd(111) system occurs at 3 ML Fe, where the structural transformation of Fe from fcc to bcc takes place. This finding is similar to the Fe/Ni/W(110) system, where the structural and spin reorientation transition occurs at 4 ML simultaneously.[19] The present results on the XMCD and the *M-H* curve analysis indicate that the stability of PMA in Fe/Ni/Pd(111) is significantly reduced from Fe 2 to 3 ML and that the second SRT takes place not only by the demagnetizing-field effect but also by some other more intrinsic origin. Although this may not be a direct relation between the spin and structural phase transitions, it should be natural to consider that the origin of the second SRT is ascribed to the structural transformation of Fe from fcc to bcc which effectively reduces the stability of PMA in terms of the orbital magnetic moments. The demagnetizing-field effect also contributes the second SRT since in our preliminary measurements the critical thickness for the second SRT is found to depend on the Ni thickness. In Fe/Ni(4 ML)/Pd(111), the second SRT was found to be completed at Fe 2.5 ML, which is slightly smaller than the one for Fe/Ni(6 ML)/Pd(111) (3.0 ML).

## IV. CONCLUSIONS

The structural and magnetic properties of Fe/Ni/Pd(111) have been investigated by LEED, MOKE, and XMCD. In the LEED measurements, incoherent growth as well as the Moiré patterns of the Ni film on Pd(111) was observed while Fe is found to grow pseudomorphically at the initial stage and to change the structure from the fcc to bcc phase around 3 ML. The magnetic easy axis of Ni/Pd(111) is in plane, irrespective of Ni thickness. Deposition of 1 ML Fe on in-plane magnetized Ni/Pd(111) induces the first SRT to perpendicular magnetization, and further deposition of 3 ML Fe causes the second SRT to in-plane magnetization. The analysis of the angle-dependent XMCD measurements reveals that the origin of the first SRT is ascribed to large PMA of the Fe-Ni interface. On the second SRT, significant reduction in the difference in the perpendicular and parallel orbital magnetic moments was found by comparing those between Fe 2 and 3 ML films, implying that the second SRT originates not only from the demagnetizing field but also from other more intrinsic reasons for the unstabilization of PMA. Since the second SRT at ~3 ML Fe coincides with the structural transformation of Fe from fcc to bcc, it is natural to consider that the second SRT to in-plane magnetization is caused by cooperative contributions of the structure transformation and the enhanced demagnetizing field.

*yokoyama@ims.ac.jp

[1] P. Bruno, Phys. Rev. B **39**, 865 (1989).
[2] H. J. Elmers, J. Hauschild, H. Höche, U. Gradmann, H. Bethge, D. Heuer, and U. Köhler, Phys. Rev. Lett. **73**, 898 (1994).
[3] J. Stöhr, J. Magn. Magn. Mater. **200**, 470 (1999).
[4] P. Gambardella, A. Dallmeyer, K. Maiti, M. C. Malagoli, S. Rusponi, P. Ohresser, W. Eberhardt, C. Carbone, and K. Kern, Phys. Rev. Lett. **93**, 077203 (2004).
[5] X. D. Ma, T. Nakagawa, Y. Takagi, M. Przybylski, F. M. Leibsle, and T. Yokoyama, Phys. Rev. B **78**, 104420 (2008).
[6] J. Li, M. Przybylski, F. Yildiz, X. D. Ma, and Y. Z. Wu, Phys. Rev. Lett. **102**, 207206 (2009).
[7] B. Schulz and K. Baberschke, Phys. Rev. B **50**, 13467 (1994).
[8] D. Pescia, M. Stampanoni, G. L. Bona, A. Vaterlaus, R. F. Willis, and F. Meier, Phys. Rev. Lett. **58**, 2126 (1987).
[9] H. Takahashi, S. Tsunashima, S. Fukatsu, and S. Uchiyama, J.

Magn. Magn. Mater. **93**, 469 (1991).
[10] D. Weller, J. E. E. Baglin, A. J. Kellock, K. A. Hannibai, M. F. Toney, G. Kusinski, S. Lang, L. Folks, M. E. Best, and B. D. Terris, J. Appl. Phys. **87**, 5768 (2000).
[11] T. Dürkop, H. J. Elmers, and U. Gradmann, J. Magn. Magn. Mater. **172**, L1 (1997).
[12] T. Yokoyama, D. Matsumura, K. Amemiya, S. Kitagawa, N. Suzudi, and T. Ohta, J. Phys.: Condens. Matter **15**, S537 (2003).
[13] H. Abe, J. Miyawaki, E. O. Sako, M. Sakamaki, and K. Amemiya, Phys. Rev. B **78**, 014424 (2008).
[14] K. W. Edmonds, C. Binns, S. H. Baker, S. C. Thornton, C. Norris, J. B. Goedkoop, M. Finazzi, and N. B. Brookes, Phys. Rev. B **60**, 472 (1999).
[15] I. M. L. Billas, A. Chatelain, and W. A. de Heer, Science **265**, 1682 (1994).
[16] H. Abe, K. Amemiya, D. Matsumura, S. Kitagawa, H. Watanabe, T. Yokoyama, and T. Ohta, J. Magn. Magn. Mater. **302**, 86 (2006).
[17] R. Ramchal, A. K. Schmid, M. Farle, and H. Poppa, Phys. Rev. B **69**, 214401 (2004).
[18] R. Thamankar, S. Bhagwat, and F. O. Schumann, J. Magn. Magn. Mater. **281**, 206 (2004).
[19] D. Sander, A. Enders, C. Schmidthals, J. Kirschner, H. L. Johnston, C. S. Amold, and D. Venus, J. Appl. Phys. **81**, 4702 (1997).
[20] T. Nakagawa, Y. Takagi, Y. Matsumoto, and T. Yokoyama, Jpn. J. Appl. Phys. **47**, 2132 (2008).
[21] T. Yokoyama, T. Nakagawa, and Y. Takagi, Int. Rev. Phys. Chem. **27**, 449 (2008).
[22] T. Gejo, Y. Takata, T. Hatsui, M. Nagasono, H. Oji, N. Kosugi, and E. Shigemasa, Chem. Phys. **289**, 15 (2003).
[23] S. Terada, T. Yokoyama, N. Saito, Y. Okamoto, and T. Ohta, Surf. Sci. **433-435**, 657 (1999).
[24] M. Wasniowska, N. J. Gilman, W. Wulfhekel, M. Przybylski, and J. Kirschner, Surf. Sci. **601**, 3073 (2007).
[25] M. F. Carazzolle, S. S. Maluf, A. de Siervo, P. A. P. Nascente, R. Landers, and G. G. Kleiman, J. Electron Spectrosc. Relat. Phenom. **156-158**, 405 (2007).
[26] P. A. P. Nascente, M. F. Carazzolle, A. de Siervo, S. S. Maluf, R. Landers, and G. G. Kleiman, J. Mol. Catal. A: Chem. **281**, 3 (2008).
[27] H. L. Johnston, C. S. Arnold, and D. Venus, Phys. Rev. B **55**, 13221 (1997).
[28] G. C. Gazzadi, F. Bruno, R. Capelli, L. Pasquali, and S. Nannarone, Phys. Rev. B **65**, 205417 (2002).
[29] B. An, L. Zhang, S. Fukuyama, and K. Yokogawa, Jpn. J. Appl. Phys. **47**, 6081 (2008).
[30] B. An, L. Zhang, S. Fukuyama, and K. Yokogawa, Phys. Rev. B **79**, 085406 (2009).
[31] F. Huang, M. T. Kief, G. J. Mankey, and R. F. Willis, Phys. Rev. B **49**, 3962 (1994).
[32] Y. Li and K. Baberschke, Phys. Rev. Lett. **68**, 1208 (1992).
[33] R. Bergholz and U. Gradmann, J. Magn. Magn. Mater. **45**, 389 (1984).
[34] Y. Takagi, K. Isami, I. Yamamoto, T. Nakagawa, and T. Yokoyama, Phys. Rev. B **81**, 035422 (2010).
[35] R. Nakajima, J. Stöhr, and Y. U. Idzerda, Phys. Rev. B **59**, 6421 (1999).
[36] J. Stöhr and H. König, Phys. Rev. Lett. **75**, 3748 (1995).
[37] J. Stöhr and H. C. Siegmann, *Magnetism*, Solid-State Sciences Vol. 152 (Springer, UK, 2006).
[38] D. Weller, J. Stöhr, R. Nakajima, A. Carl, M. G. Samant, C. Chappert, R. Mégy, P. Beauvillain, P. Veillet, and G. A. Held, Phys. Rev. Lett. **75**, 3752 (1995).